IIETA International Information and Engineering Technology Association
Advancing the World of Information and Engineering

Journal Européen des Systèmes Automatisés
Vol. 58, No. 7, July, 2025, pp. 1315-1325
Journal homepage: http://iieta.org/journals/jesa

Toward Smart Factories: Modelling Hybrid RF and VLC Communication Channels for IIoT Applications

Ameur Chaabna[1*], Takoua Hafsi[2], Abdesselam Babouri[3], Zine Eddine Meguetta[4], Mohamed Benrabah[1], Halim Chouabia[3], Xun Zhang[5]

[1] LRPE Laboratory, Department of Automation, University of Science and Technology Houari Boumediene, Algiers 16111, Algeria
[2] LAM2SIN Laboratory Annaba, Department of Mathematics, University of Science and Technology Houari Boumediene, Algiers 16111, Algeria
[3] LGEG Laboratory, Department of Electrical Engineering and Automation, Université 8 Mai 1945 Guelma, Guelma 24000, Algeria
[4] Enseignant BTS Eléctronique et Informatique Cyber Sécurité, Campus Supérieur Lycée Frédérique Ozanam, Lille 59000, France
[5] Institut Supérieur d'Electronique de Paris (ISEP), Paris 75006, France

Corresponding Author Email: ameur.chaabna@usthb.edu.dz

https://doi.org/10.18280/jesa.580701

Received: 1 June 2025
Revised: 4 July 2025
Accepted: 16 July 2025
Available online: 31 July 2025

Keywords:
hybrid channel, IIoT, light fidelity Li-Fi, RF channel, smart factory, Visible Light Communication (VLC), Wi-Fi

ABSTRACT

LED lighting technology has gained wide popularity in recent years. Visible Light Communication (VLC) stands to become an excellent replacement medium for indoor high-speed Internet and Industrial Internet of Things (IIoT). This work aims to model a hybrid wireless communication system, where a visible light channel and a radio frequency (RF) channel work together to form a Multiple Input Multiple Output (MIMO) system. Combining optical and RF communication channels can boost data rate as optical devices have higher bandwidths. The analysis is conducted by examining the application of collaborative robots (Cobots). VLC links will direct downwards from ceilings (downlink) to deliver data as well as illumination. However, shining lamps upwards (uplink) will produce an uncomfortable glare. RF can not only provide the uplink, but it can also improve stability and speed if it operates together with VLC. Many principles, like frequency reuse plan and Shannon spectral efficiency, have been applied to enhance and improve our results. This study investigates the Bit Error Ratio (BER) in OOK modulation, multi-user access, received power distribution, and hybrid VLC/Wireless Fidelity (Wi-Fi) networks. Clear advantages can be seen, particularly in critical areas where traditional RF communications may pose security risks or suffer from interference.

1. INTRODUCTION

Wireless network access has no end. The development of IIoT devices will continue to increase demand for wireless access networks [1]. The ongoing transformation towards the industrial metaverse extends and expands the domain of communication beyond traditional IIoT applications. This transformation changes what can be connected and how we create and interact with Immersive Virtual Environments (IVE) compared to the current approach, under the line of advancement of technologies such as Artificial Intelligence (AI) [2]. The physical and digital realms merging, that's the heart of the industrial metaverse, and we're seeing unprecedented collaboration, innovation, and interaction across boundaries of distance and discipline.

One crucial factor in taking this step is the improvement of communication between Programmable Logic Controllers (PLCs) and robots, to form independent and interoperable networks. These networks enable near-autonomous data sharing between things and virtual worlds with reduced or no human interaction [3].

Intelligent systems and devices that transfer, process, and respond to information in real-time are the key to this integration. Of these, Cobots shine as representative examples. Intended to work in collaboration with people in physical and virtual worlds, Cobots represent the integration of cyber-physical systems that can enhance the efficiency and safety of deployment [4]. Nevertheless, operating such platforms in regulated settings with strict data privacy and security requirements necessitate a more in-depth analysis of IIoT implementation tactics for compliance guarantee.

Wi-Fi, Bluetooth Classic, and Bluetooth Low Energy (BLE) technologies are commonly utilized in everyday applications. However, in indoor locations with a high density of mobile devices, the RF band will become saturated, and Wi-Fi users will frequently experience significant contention and interference. To address this issue, new technologies like VLC can be employed. VLC is expected to become the next

complementary medium for indoor high-speed Internet and IIoT applications [5]. It enables the usage of energy efficient lighting luminaries [6], particularly the Light Emitting Diodes (LEDs) as high-speed data Access Points (APs) offers a complement to RF, the bandwidth of light is virtually unlimited. Local power-line infrastructure can be used as backbone [7-9]. The deployment of VLC is an excellent solution for indoor environments such as high-security smart buildings where high-speed data is communicated via modulation [10].

An aggregated Wi-Fi/VLC system combining a Wi-Fi and a VLC link was previously demonstrated in the study [11]. The overall aim of the study [12] is not merely to point out the most effective communication protocols for Cobot interaction but also to establish a foundational framework for specific applications and spearhead future innovations in IIoT applications. The authors [13] concentrate on upgrading the traffic system for the Intelligent Transportation System (ITS). In the study [14], the authors describe a light fidelity (Li-Fi)/femtocell hybrid network system for indoor environments. In the study [15], an indoor hybrid system that combines Wi-Fi and VLC luminaires was developed. It employs (1) broadcast VLC channels to supplement RF communications, and (2) a handover mechanism between Wi-Fi and VLC to dynamically divide resources and improve system throughput.

A natural downlink is typically provided by lights installed on the ceiling. Therefore, the uplink remains one of the most significant challenges in VLC. Transmitting data via VLC toward the ceiling is generally considered impractical. It also causes discomfort. One of the solutions is to shift the VLC emitter and receiver from the ceiling to the walls, but this would also affect the interior design of the environment [16]. Li-Fi is a subclass or specialized implementation of VLC that allows for high-speed, two-way, networked wireless communication via visible light.

In this work, a hybrid communication system is proposed to solve the uplink problem: that is, to use RF as the uplink, and VLC and RF as the downlink. The authors focus mainly on the modelling of the optical wireless channel and the conventional radio-wave wireless channel for IIoT. It is highly expected that future smartphones will include a VLC transceiver. Therefore, a combined mathematical model that utilizes both the VLC and Wi-Fi channels simultaneously to achieve high-speed data transfer and support the evolving demands of industrial automation is proposed.

The remainder of this paper is organized as follows: In Section 2, the proposed industrial environment modelling for smart manufacturing is described. In Section 3, the Hybrid VLC/RF channel Modelling in Industry 4.0 is presented under Co-Channel Interference (CCI) and with Non-Co Channel Interference (N-CCI) Conditions. Section 4 discusses and evaluates the performance of the proposed system conducted BER analysis in OOK modulation, multi-user access, received power distribution, and hybrid VLC/Wi-Fi channels. Finally, a conclusion is given in Section 5.

2. INDUSTRIAL ENVIRONMENT MODELING FOR SMART MANUFACTURING

As a use-case in the real world, we characterize a MIMO system in a standard-sized room measuring 7 m × 7 m × 3 m. Four LED sources are mounted on the ceiling, and the receiving plane is located at a height of 0.85 m, and a Wi-Fi wireless router is located on a wall very close to the ceiling, as shown in Figure 1. A communication system is established between a PLC and a Cobot in an IIoT context, where machine-to-machine interaction with wireless communication is emphasized. The apparatus shown in Figure 1 is used to emulate Cobot control in a controlled environment, in contrast to direct Ethernet control with a PC, for better flexibility. Cobots are employed in IIoT applications due to their flexibility, data-augmentation capabilities, productivity, and safety of the human-partner, making the work easier and safer [4]. For manufacturing, when the need for distance and special protective equipment is removed, Cobots become a very interesting tool for a factory with a wide reach.

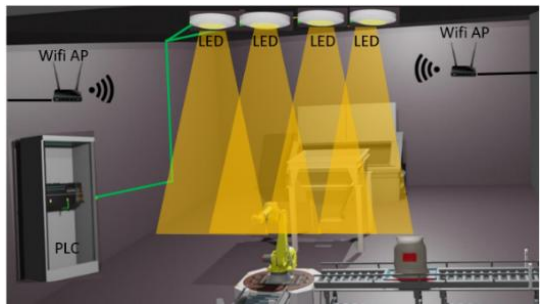

Figure 1. Industrial IOT scenario of the proposed system

Indoor channels correspond to narrow coverage regions within industrial environments, including smart factories. Because they are totally enclosed by walls, the Power Azimuth Spectrum (PAS) is uniform (i.e., the scattered components from all directions have roughly the same power) [17]. Considering that the terminals' internal mobility is modest, the channel is relatively static. The next-generation wireless network needs a combined radio frequency and visible light signalling and transmission model. The proposed VLC-RF channel is basically for MIMO channels.

By integrating both channels, we will be able to predict and improve the signal quality and capacity indoors and maximize the usage of all the possible communication devices by integration (i.e., using RF as the uplink, and RF and VLC as the downlink). The proposed hybrid channel is illustrated in Figure 2.

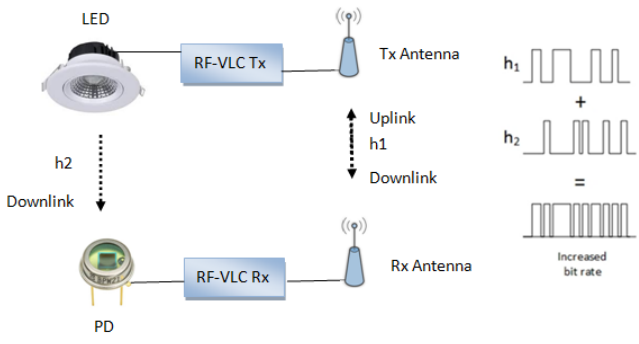

Figure 2. RF-VLC communication hybrid channel

3. HYBRID VLC/RF CHANNEL MODELLING IN INDUSTRY 4.0

According to the study [18], the LED optical Line of Sight (LOS) channel is characterized by Eq. (1) as follows:

$$H(0)_{LOS} = \begin{cases} \frac{m+1}{2\pi d^2} A \cos^m(\phi) \cos(\psi), 0 \le \psi \le \psi_c \\ 0, \qquad \psi > \psi_c \end{cases} \quad (1)$$

where, A denotes the active area of the photodiode, ψ represents the incidence' angle relative to the receiver axis, ψ_c defines the detector's Field of View (FOV), d refers to the distance separating the transmitter and the receiver, and ϕ denotes the angle of irradiance measured relative to the transmitter's perpendicular axis. The Lambertian order m is expressed as $m = \frac{-\ln 2}{\ln\left(\cos \phi_{\frac{1}{2}}\right)}$ where the half power angle of the LED is given by $\phi_{\frac{1}{2}}$.

The total optical power of *i* LEDs is given in Eq. (2):

$$P_{rx,LOS} = \sum_{i=1}^{LEDs} P_{tx} H_{LOS}^{i}(0) \quad (2)$$

where, H_{LOS}^{i} is $i-th$ LED channel DC gain, P_{tx} is the transmitted optical power from LED.

We utilize the same strategy for modelling optical wireless non-Line of Sight (NLOS) signals as used for the sphere model [16]. In a room, the first diffuse reflection of a wide-beam optical source emits an intensity I_1 over the entire surface A_{room}, as described by Eq. (3).

$$I_1 = \rho_1 \frac{P_{totalLED}}{A_{room}} \quad (3)$$

where, the reflectivity of the surface and the total power of all the LEDs are expressed by ρ_1 and $P_{totalLED}$, respectively.

The average reflectivity $< \rho >$ is defined by Eq. (4).

$$< \rho >= \frac{1}{A_{room}} \sum_i A_i \rho_i \quad (4)$$

where, $< \rho >$ denotes the area-weighted reflectivity of the ceiling, walls, floor, and other objects in the room, with A_i representing their respective surface areas.

As a result, the total intensity is calculated in Eq. (5) by summing a geometric series.

$$I = I_1 \sum_{j=1}^{\infty} < \rho >^{j-1} = \frac{I_1}{1 - < \rho >} \quad (5)$$

Such as the reflections number is expressed by *j*.

Considering the receiver as a small surface element within the room, the NLOS received power P_{NLOS} and its corresponding area A_{rx} are provided in Eq. (6).

$$P_{NLOS} = A_{rx} I \quad (6)$$

Therefore, the NLOS channel loss is defined by Eq. (7):

$$\eta_{NLOS} = \frac{P_{NLOS}}{P_{totalLED}} = \frac{A_{rx}}{A_{room}} \frac{\rho_1}{1 - < \rho >} \quad (7)$$

3.1 Superposition of LOS and NLOS channels

The received power is given by:

$$P_{rx} = \left(P_{LOS} + P_{NLOS}\right) * T_s(\psi) * g(\psi) \quad (8)$$

Such as the gain of the optical filter and the gain of the optical concentrator are expressed by $T_s(\psi)$ and $g(\psi)$, respectively.

Therefore, according to Eq. (9), the gain of combined channel [19] is given as follows:

$$H_{NLOS+LOS}(f) = H(0)_{LOS} + H_{NLOS}(f) e^{j2\pi f \Delta T} \quad (9)$$

where, ΔT is the delay between the onset of the NLOS signal and the LOS signal.

The gain of the optical concentrator $g(\psi)$ is given by [20]:

$$g(\psi) = \begin{cases} \frac{\eta_c^2}{\sin^2(\psi_c)}, & 0 \le \psi \le \psi_c \\ 0, & \psi > \psi_c \end{cases} \quad (10)$$

where, η_c denotes the concentrator refractive index.

In this system, optical OOK-NRZ modulation is employed. The block diagram of OOK system is illustrated in Figure 3.

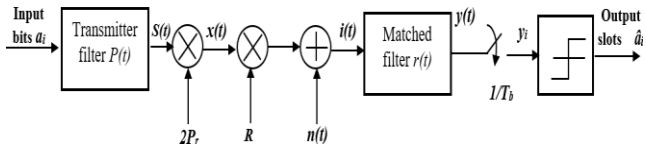

Figure 3. Block diagram of OOK system

The OOK-NRZ modulation envelop is given by Eq. (11).

$$p(t) = \begin{cases} 2P_r & for \quad t \in [0, T_b) \\ 0 & elsewhere \end{cases} \quad (11)$$

where, the average power is expressed by P_r and the bit duration is denoted by T_b.

3.2 Bit error rate (BER)

The probability of error is given as:

$$P_e = p(1) \int_0^{i_{th}} p(i/1) di + p(0) \int_{i_{th}}^{\infty} p(i/0) di \quad (12)$$

where, the level of threshold is presented by i_{th}, *P(1)* and *P(0)* denote probabilities of 'one' and 'zero', while Eq. (13) defines the marginal probabilities.

$$p(i/0) = \frac{1}{\sqrt{2\pi\sigma^2}} exp\left(\frac{-i^2}{2\sigma^2}\right)$$
$$p(i/1) = \frac{1}{\sqrt{2\pi\sigma^2}} exp\left(\frac{-(i - I_p)^2}{2\sigma^2}\right) \quad (13)$$

Assuming equally probable symbols, i.e., *P (0) = P (1) = 0.5*, the optimal decision threshold is given by $i_{th} = 0.5 I_p$,

leading to a simplified expression for the conditional probability of error:

$$P_e = Q\left(\frac{i_{th}}{\sigma}\right) \tag{14}$$

where, Marcum's Q-function is expressed by $Q()$, it is the area under the Gaussian curve, it can be computed by Eq. (15).

$$Q(x) = \frac{1}{\sqrt{2\pi}} \int_x^{\infty} e^{-\alpha^2/2} d\alpha \tag{15}$$

When using a matched filter, the output noise variance is entirely governed by the power spectral density (PSD) of the input noise and the total energy of the filter's impulse response. Consequently, if the input noise is additive white Gaussian noise (AWGN) with a double-sided PSD of $N_0/2$, the resulting noise variance at the output of the matched filter can be expressed using Eq. (16).

$$\sigma^2 = \frac{N_0}{2} \int_{t=0}^{T_b} r^2(t) dt \tag{16}$$

The standard deviation, noted by σ, can be computed using Eq. (17) and Eq. (18), while the average energy per bit E_b is given by Eq. (19).

$$\sigma = \sqrt{\frac{N_0 E_p}{2}} \tag{17}$$

$$P_{e\_bit\_OOK} = Q\left(\sqrt{\frac{E_b}{N_0}}\right) \tag{18}$$

$$E_b = \frac{E_p}{2} = 2\left(RP_r\right)^2 T_b \tag{19}$$

In the case of OOK-RZ formatting, E_b is increased by a factor of $\frac{1}{\gamma}$ according to Eq. (20) as follows.

$$E_b = \frac{E_p}{2} = \left(2\left(RP_r\right)^2 T_b / \gamma\right) \tag{20}$$

The Signal-to-Noise Ratio (SNR) can be introduced as [21]:

$$SNR_{\mu,r}(f) = \frac{\left|G_{\mu,\alpha}(f)\right|^2 P_R}{\sigma^2}, \tag{21}$$

where, the subcarrier transmits power, the variance of additive white Gaussian noise (AWGN), and the channel gain are expressed by P_R, σ2, and $G_{\mu,\alpha}(f)$, respectively. In VLC, for user μ and AP α, the Signal-to-Interference-plus-Noise Ratio (SINR) is expressed as [22]:

$$SINR_{\mu,r} = \frac{(\kappa P_{tx} H_{\mu,\alpha})^2}{N_0 B + \sum (\kappa P_{tx} H_{\mu,else})^2}, \tag{22}$$

Here, κ denotes the conversion optical to electrical efficiency at the receiver side; The noise power spectral density is represented by $N_0[A^2/Hz]$; $H_{\mu,\alpha}$ refers to the gain of the channel between the associated VLC AP and user μ; and $H_{\mu,else}$ denotes the gain of the channel between the interfering VLC AP and user μ; and the LED modulation bandwidth is expressed by B.

3.3 Radio frequency communication channel

Considering an indoor environment where emitters and receivers are more or less stationary, the wireless RF channel can be commonly characterized by [23]:

$$h(\tau) = \sum_i a_i \delta(t - \tau_i) \tag{23}$$

where, a_i and τ_i are the attenuation and propagation delay associated with the i^{th} multipath component, respectively. δ is the data function.

According studies [24, 25] the indoor path loss in buildings was carefully studied. Although the same three mechanisms (reflection, diffraction, and scattering) are dominated in indoor and outdoor environments, indoor conditions are much more variable. For example, the signal does vary levels greatly in case of opened and closed doors. Also, the position of Wi-Fi antennas has an important impact on receiving signal.

We will only consider losses by hard partitions (e.g., concrete walls and floors which are part of the building structure). They have physical and electrical characteristics which will affect radio paths. For example [26], a concrete wall has been measured to have about 8-15 dB losses, while a concrete floor has a 10 dB loss. In addition, the external dimensions, the building materials and building technology determine losses between floors. The Floor Attenuation Factor (FAF) typically ranges from 13 to 45 dB [17].

Indoor path loss obeys the distance power law. According to the study [27], the loss model can be expressed using Eq. 24 in the case where walls are in a direct path between receiver and transmitter antennas.

$$L(d) = L_0 + 10n \log d + kF_1 + \sum_{i-1}^{M} A_i \tag{24}$$

Such as M denotes the partitions number between receiver and transmitter antennas, A_i presents the attenuation factor for the i^{th} partition, $L(d)$ indicates the path loss over distance d from the transmitter, L_0 denotes the propagation attenuation of free space over a reference distance of 1 m, n is the path-loss exponent, k presents the number of floors between transmitter and receiver antennas and F_1 is the single-floor propagation attenuation (floor loss factor).

3.4 Hybrid VLC-RF channel

Since noise components Z_{vlc} and Z_{rf} are independent, the information capacity of the total channel is expressed ~~as~~ in Eq. (25):

$$C = \max_{p\left(x_{vlc}, x_{rf}\right) \cdot \sum_{j=1}^{k} p_j \le p} I\left(X_{vlc}, X_{rf}, Y_{vlc}, Y_{rf}\right)$$

$$= \max_{\{p_j\} s.t. \sum p_j \le p} \sum_{j=1}^{k} \frac{1}{2} log\left(1 + \frac{P_j}{\sigma_j^2}\right) \quad (25)$$

Which is achieved if $(X_{vlc}, X_{rf}) \sim \aleph\left(0; dig\left(P_{vlc}, P_{rf}\right)\right)$.

Lagrange multipliers can be used to solve the power allocation problem since it simplifies to a typical optimization problem.

$$\max_{P_j} \sum_{j=1}^{k} log\left(1 + \frac{P_j}{\sigma_j^2}\right) \quad (26)$$

$$subject \quad to \sum_{j=1}^{k} P_j = P, \left(P_j \ge 0\right) \quad (27)$$

where, U is chosen subjected to $\sum_j P_j \le P$. If channel j is allocated, then its power will be $P_j = U - \sigma_j^2$; otherwise, $P_j = 0$. Power is allocated to the channel with the lowest variance, and as the power budget grows, we fill the channels in order of increasing noise variances. At any given time, the total of noise variance and signal strength in the channels in use is U.

3.5 Total received power

The total received power is calculated by:

$$P_{RT}\left(dB\right) = P_{RLED}\left(dB\right) + P_{RRF}\left(dB\right) - Loss_{RF}\left(dB\right) \quad (28)$$

The received RF power is calculated without including the VLC channel as given in:

$$P_R\left(dB\right) = P_{RRF}\left(dB\right) - Loss_{RF}\left(dB\right) \quad (29)$$

where, P_{RLED} is the received power of the LED channel in Eq. (8); P_{RRF} is the received power and $Loss_{RF}$ is the total loss mentioned in Eq. (24). Referring back to Figure 2, Eq. (28) is used for the downlink, while Eq. (29) is used for the uplink.

3.6 Load balancing and dynamic handover

Due to the small coverage area of VLC LEDs, the movement of users can probably prompt handover. A handover happens when a user's serving AP switches between two nearby states. In general, the handover overhead in an indoor environment is in the millisecond range, which is believed to be less than the state interval T_p [21]. The handover efficiency between two nearby states is defined according to Eq. (30) as follows:

$$\eta_{i,j} = \begin{cases} \left[1 - \frac{t_{i,j}}{T_p}\right]^+, & i \ne j \\ & i, j \in C \\ 1, & i = j \end{cases} \quad (30)$$

Such as $t_{i,j}$ presents the overhead of AP switch from AP_i to AP_j. The link data rate between AP α and user μ in state n with handover efficiency is given by Eq. (31).

$$r_{\mu,\alpha}^{(n)} = \begin{cases} \eta_{\alpha'\alpha} R_0, & \alpha = 0 \\ \eta'_{\alpha'\alpha} R_{\mu,\alpha}^{(n)}, & \alpha = 1,2...N_c \end{cases} \quad (31)$$

where, $R^{(n)}{}_{\mu}$ denotes the data rate of VLC, α' presents the AP of user μ in the state $n-1$, η′ describes the handover efficiency from AP α′ to AP α, and R_0 gives the Wi-Fi throughput.

The load balancing algorithm used in each state is expressed using Eq. (32) as follows:

$$\gamma_\beta(x) = \begin{cases} log(x), & \beta = 1 \\ \frac{x^{1-\beta}}{1-\beta}, & \beta \ge 0, \quad \beta \ne 1 \end{cases} \quad (32)$$

where, the proportional coefficient is denoted by β. In particular, the maximal system throughput is reached when $\beta = 0$ and a linear utility function is realized; proportional fairness is attained when $\beta = 1$; and max-min fairness is attained when $\beta \to \infty$ [21].

4. RESULTS AND DISCUSSION

4.1 Bit Error Ratio

The modulation scheme employed in this work is On-Off Keying with Non-Return-to-Zero encoding (OOK-NRZ). Path loss and multipath dispersion effects are neglected. The noise is assumed to be white and Gaussian, to focus on analysing the probability curve of OOK and comparing simulation results with theoretical results. The block diagram for the BER calculation is shown in Figure 4.

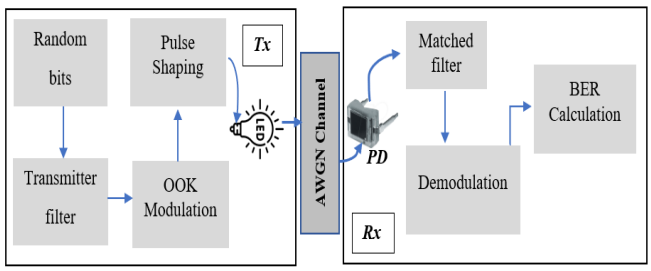

Figure 4. Block diagram of BER calculation

The main parameters used in this simulation are mentioned in Table 1.

Table 1. OOK modulation parameters

Parameters	Values
Charge of electron	$q=1.6\ e^{-19}$
Background noise current	$I_b=202e^{-6}$
Noise spectral density	$N_0=2*q*I_b$
Bit rate	$R_b=1e^6$
Bit duration	$T_b=1/R_b$
Number of bits	sig_length=$1e^5$
Samples per symbols	nsamp=10

An analysis of the BER as a function of SNR with theoretical and simulation results is shown in Figure 5. A filter is applied to the transmitted signal, and a matched filter is used at the receiver side in this simulation. Based on these principles, the randomly generated transmitted signal is effectively matched at the receiver. Additionally, rectangular

pulse shaping is applied on both the transmitter and receiver sides to enable convolution of the received pulses. At the detection stage, a digital symbol '1' is assumed to be received if the signal exceeds a predefined threshold level, and '0' otherwise. The main objective of this simulation process is to minimize errors that may occur during transmission. As a result, the simulated and theoretical BER curves are nearly identical.

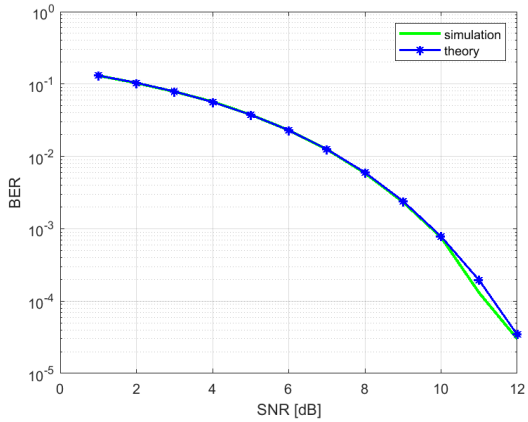

Figure 5. BER vs SNR plot for OOK modulation

4.2 Multiple access techniques for VLC systems

As a wireless broadband technology, VLC can provide simultaneous network access to many users. In this section, four simulations are run to test that ability using four multiple access methods: Frequency Division Multiple Access (FDMA), Time Division Multiple Access (TDMA), Non-Orthogonal Multiple Access (NOMA), and Spatial Division Multiple Access (SDMA).

4.2.1 Performance evaluation of multiuser access in VLC attocell architecture

Figure 6 shows the simple idea of downlink NOMA. Here, the LED sends out a joint signal which has messages meant for many users. This signal is created by adding up the separate user signals and making each one larger or smaller using a certain weighting factor. This way, known as power-domain multiplexing, it lets many users share the same sending channel in a good way [28].

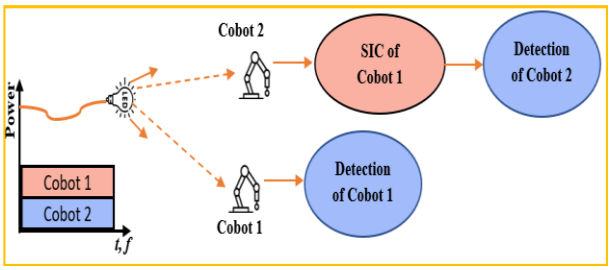

Figure 6. Illustration of the NOMA principle by a two-Cobots scenario

Figure 6 illustrates the operation of the Successive Interference Cancellations (SIC) as a receiver-side post-processing stage to remove the Inter-User interference. In NOMA techniques, SIC is used to mitigate interference, supported by a Transmission Control Protocol (TCP) vector and SDMA.

Figure 7 shows a comparison of FDMA and NOMA in a VLC attocell with two users shown as an example. Based on Shannon's spectral efficiency and the results shown in the figure, NOMA offers much better performance than sum throughput within the VLC LED.

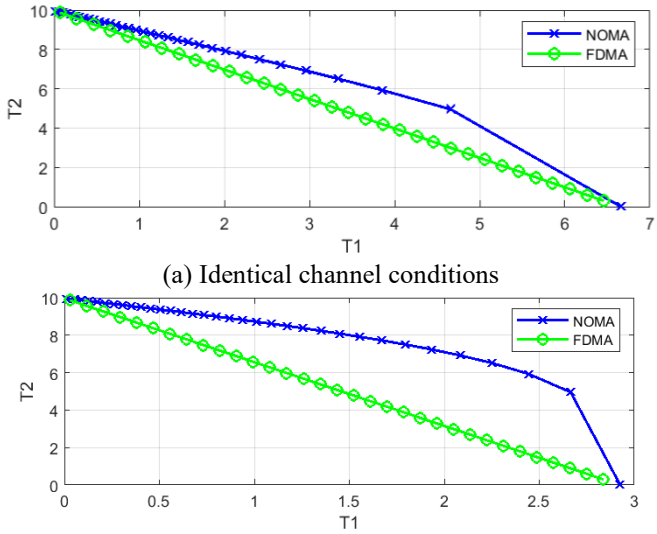

(a) Identical channel conditions

(b) Distinct channel conditions

Figure 7. Shannon spectral efficiency of NOMA vs. FDMA

This work compares FDMA with NOMA. The difference in the access schemes notwithstanding, both studies yield similar conclusions. This is basically because both TDMA and FDMA depend on user-scheduling mechanisms making an effort to be fair in allocating resources. The main contribution of our work is to clearly put in evidence that NOMA can achieve a much better overall VLC throughput especially for multiple users. This emphasizes the ability of NOMA to beat conventional methods like FDMA and TDMA in terms of spectral efficiency and user capacity in the VLC systems.

4.2.2 Multiuser communication in VLC attocell networks

The utilization of TDMA, NOMA and SDMA in a VLC network is studied in the context of overlapping coverage of adjacent VLC AP, as plotted in Figure 8. It has been observed in [28] that NOMA directly employed in these scenarios does not help resolve the interference caused by neighbouring attocell. A potential and effective method to optimize the performance of the edge users with respect to the centralized base station (CBS) users is the combination of NOMA with SDMA, which exploits the separation in space domain so as to improve signal quality and mitigate inter-cell interference.

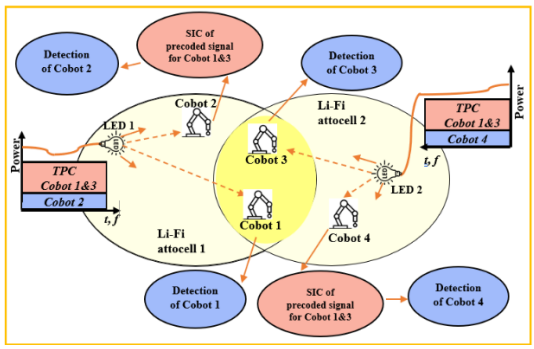

Figure 8. Illustration of NOMA and SDMA integration for two LEDs

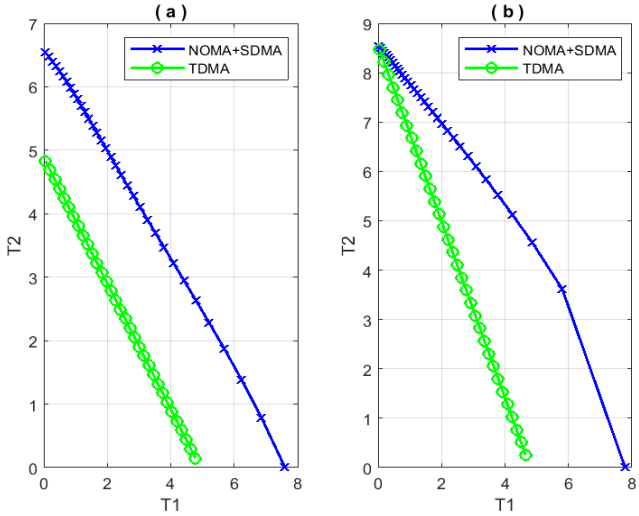

Figure 9. Spectral efficiency comparison of NOMA/SDMA vs. TDMA in VLC:(a) Both users at LED edge;(b) One at edge, one at centre

Figures 9(a) and 9(b) results show a performance comparison of TDMA with the hybrid SDMA/NOMA scheme in a VLC network considering two users' scenario having one user in the overlapping region between the adjacent attocell based on Shannon's spectral efficiency since it is indicated that combined SDMA/NOMA offers much better throughput performance where there is interference, outperforming TDMA and FDMA in overall capacity of the VLC system.

4.2.3 Integration of VLC and Wi-Fi for hybrid wireless communication

Due to the increasing need for fast wireless data transmission and the tightening radio spectrum, a combined VLC/Wi-Fi shall take much popularity in the upcoming years. This shall be the major step toward the general use of VLC.

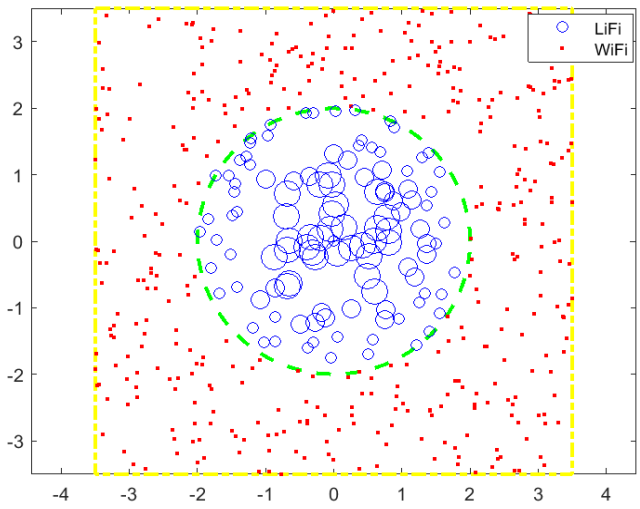

Figure 10. SNR distribution in a VLC access point

SNR Analysis in a Hybrid VLC/Wi-Fi System Using One LED. This simulation deals with the SNR distribution in a VLC LED illuminated by one LED. Note that the size of the blue circles in the simulation pictures varies according to the SNR levels within the coverage area.

Figure 10 demonstrates the SNR distribution across a VLC LED, which is the basis for the following reasoning. From the results, it can be observed that the SNR is maximum near the centre of the cell for small radial distances *r*. This observation also coincides with the findings from the application of Shannon's capacity theorem in consideration of the distance of each user from the VLC AP. Increase in distance r results in gradual negative change in SNR which decreases to 0 dB at the boundary of the cell. After this point, VLC does not serve the users and they are switched over to Wi-Fi.

Four LEDs Hybrid VLC/Wi-Fi System with N-CCI. In this case, a hybrid system consists of four VLC LEDs with N-CCI conditions. The objective is to investigate the impacts of different levels of Wi-Fi throughput on mobility and connectivity for each VLC LED.

Figure 11 shows when Wi-Fi throughput is set to 120 Mbps and in Figure 12, it is set to 1 Gbps. These are the values showing performance fluctuations due to varying Wi-Fi throughput under N-CCI.

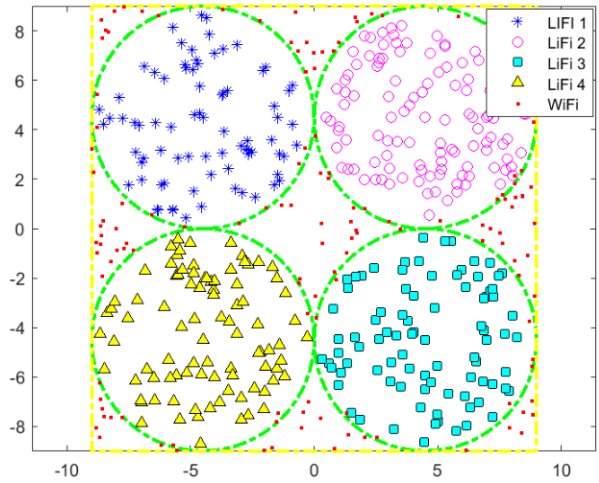

Figure 11. Users' coverage pattern in N-CCI scenario with Wi-Fi throughput of 120 Mbps

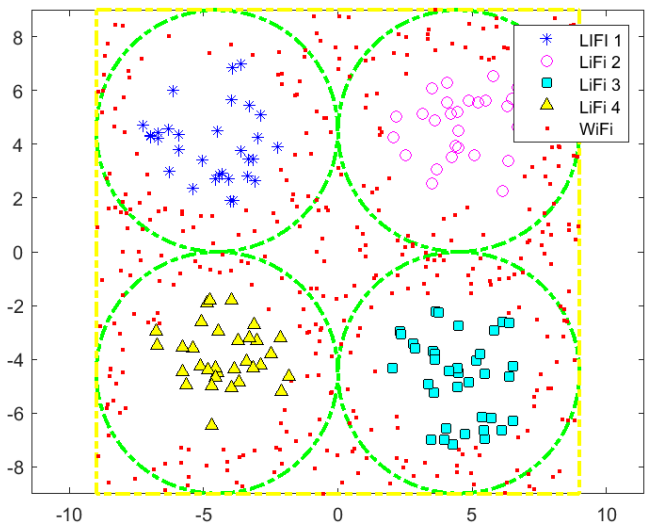

Figure 12. Users' coverage pattern in a N-CCI situation with Wi-Fi data rates of 1 Gbps

The obtained results, study the effect of Wi-Fi throughput in N-CCI case with four VLC AP. The results support the first hypothesis, due to SNR distribution as shown in Figure 10, near the edge of each VLC LED the SNR approaches zero.

Users who are hence in these low-SNR zones are covered by the Wi-Fi network. With increasing Wi-Fi throughput, the number of edges connected users offloaded to Wi-Fi increases until it approaches the stage when Wi-Fi throughput is approximately equal to VLC throughput.

As we see in Figure 12, in case of Wi-Fi throughput being 1 Gbps, users located at the edges of VLC LEDs are served by Wi-Fi. This is because, at the edges, the VLC SNR is lower relative to the signal strength provided by Wi-Fi which provides much greater throughput in this scenario.

Hybrid VLC/Wi-Fi system with two VLC LEDs under CCI conditions. The focus of this section is the evaluation of a hybrid VLC/Wi-Fi system under the CCI scenario with the overlap of two VLC LEDs. The study analyses the following three parameters: SNR distribution within VLC LEDs, the effect of Wi-Fi throughput, SINR. These factors together determine the effective number of users supported by each VLC AP.

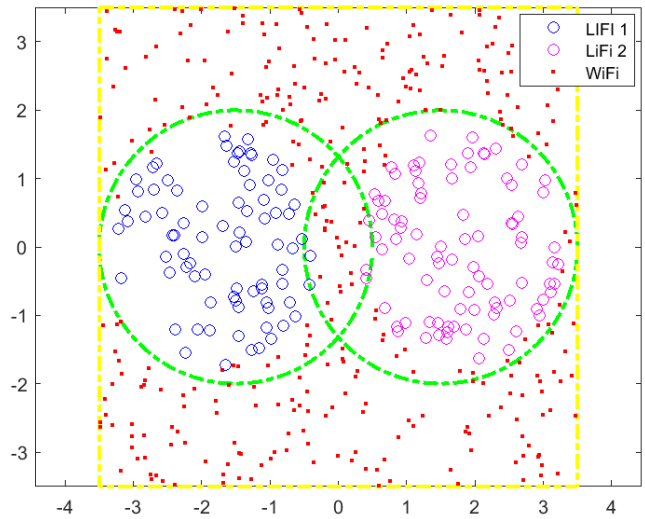

Figure 13. Users' coverage pattern in CCI scenario

This section aims to study the impact of the overlapping region on user allocation and network service distribution while focusing on the impact of SINR. The spatial user distribution in and out of the region of overlap is illustrated in Figure 13 alongside the cell intersection layer showing the cross-section region performance.

The findings indicate that users situated within the overlapping region suffer degraded SINR due to excessive interference. As a result, these users tend to be served by the Wi-Fi network which benefits them with greater SNR and throughput under these conditions.

Hybrid VLC/Wi-Fi system with four VLC LEDs under CCI conditions. This simulation has taken VLC and Wi-Fi throughputs to be 1 Gbps. Figure 14 presents the perspective of user distribution and performance affected by CCI, based on SNR and SINR values.

The findings are summarized as: users in the overlapping regions between VLC LEDs are primarily served by the Wi-Fi network due to higher SNR and lowered SINR in those regions. VLC channels are kept through impairing-free regions with enough SINR for maintaining reliable communication, and with the increasing of Wi-Fi throughput, the number of VLC-served users decreases, as Wi-Fi becomes more favourable in areas with low VLC SNR.

Frequency reuse techniques in a hybrid VLC/Wi-Fi system. In all previous simulations for the hybrid VLC/Wi-Fi network, it was assumed that the Wi-Fi configuration had been set to near-maximum throughput under fewer than 12 meters to facilitate a modelling process. In this section, we examine a more realistic situation in which the Wi-Fi coverages are limited or degraded while four VLC LEDs suffer from CCI conditions so as to serve more users for VLC within their overlapping coverage areas.

Frequency reuse techniques are thus introduced to diminish the interference between cells and hence improve the usefulness of VLC.

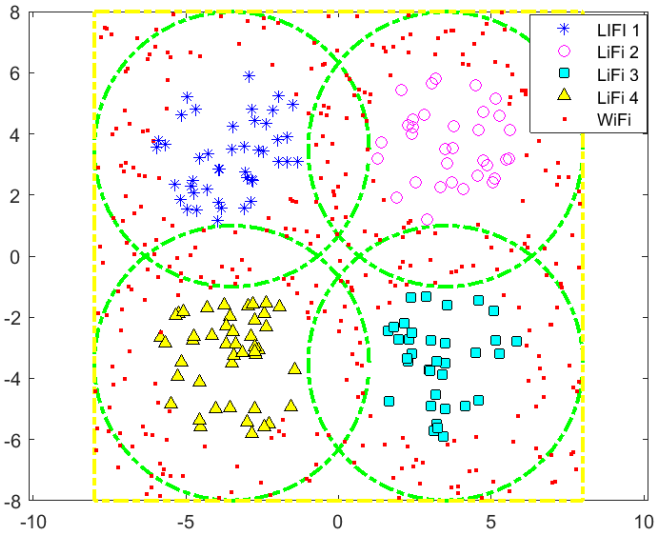

Figure 14. Users' coverage pattern in CCI scenario with Wi-Fi throughput of 1Gbps

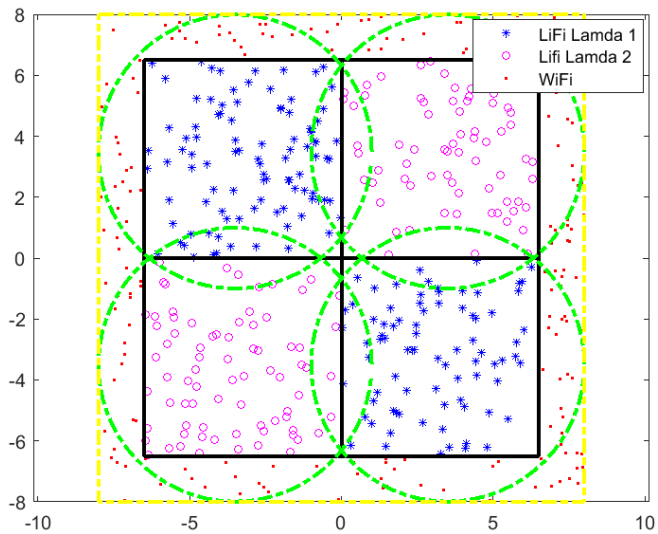

Figure 15. Impact of frequency reuse plan on users' distribution

Figure 15 shows how frequency reuse is employed in the VLC network. The total bandwidth of a white LED, assumed to be 20 MHz, is split among the cells. Since there are four intersecting VLC LEDs, spectrum allocation is done in a way to try to minimize interferences, in effect creating frequency zones that remain separate from each other. The simulation analysis shows that the total amount of VLC users increases. The structured frequency planning alongside square-shaped cell layouts prevents Wi-Fi users from accessing VLC

coverage zones despite the reduced bandwidth per cell which leads to decreased VLC throughput. The risk of inter-cell interference is completely eliminated in this approach.

4.2.4 Power distribution

The received power distribution at the receiver plane for an industrial environment measuring 7 × 7 meters appears in Figure 16. The power distribution from a single transmitter appears in Figure 16(a) while the corresponding optical channel gain appears in Figure 16(b). Four transmitters produce a more consistent optical power distribution across the room than a single-transmitter setup as shown in Figures 16(a) and 17(a).

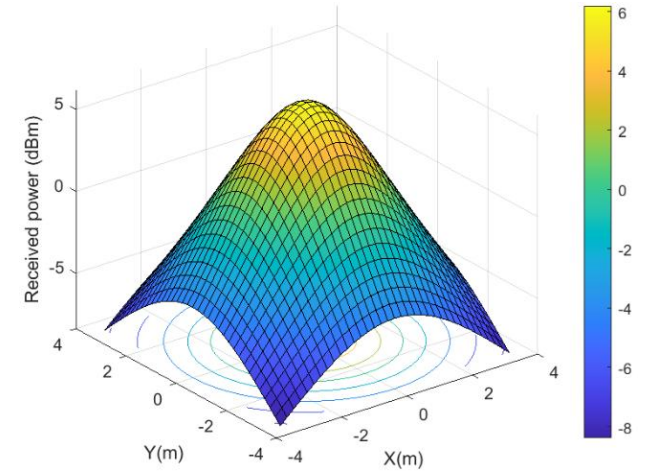

(a) Received power for one transmitter

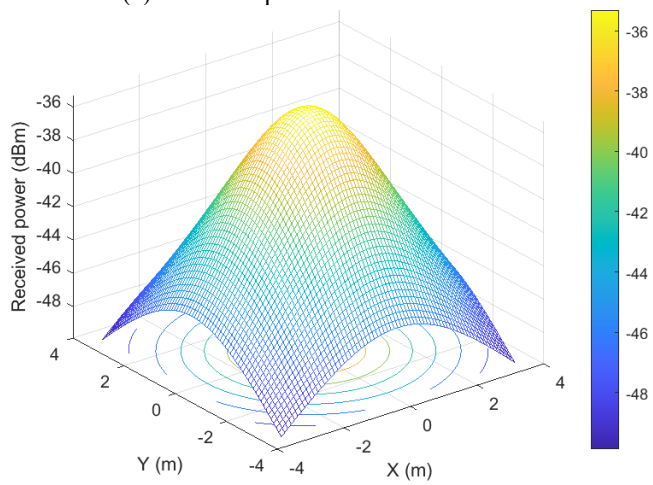

(b) Channel gain for one transmitter

Figure 16. Received power distribution

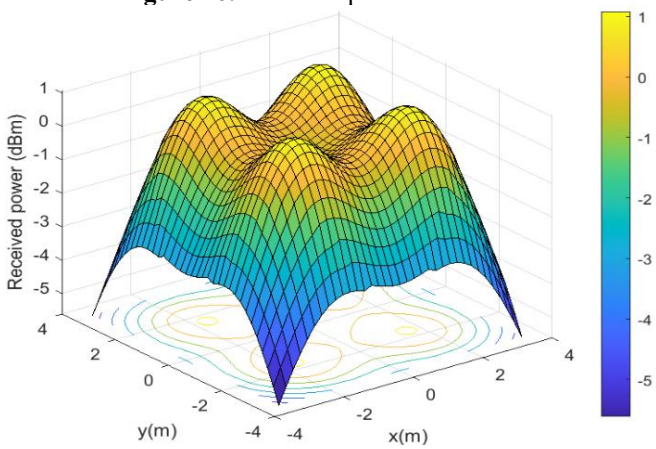

(a) $\phi_{\frac{1}{2}} = 70°$

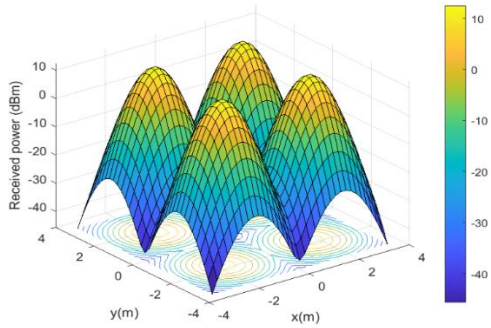

(b) $\phi_{\frac{1}{2}} = 12.5°$

Figure 17. Received power with four transmitters

Figures 17(a) and 17(b) analyse the power distribution when four transmitters operate with different half power angle of the LED. The received power strength at the receiver is higher for the 12.5° half power angle than for the 70° wide angle as demonstrated by the comparison of Figures 17(a) and 17(b). The data shows that tighter angles improve power reception because they minimize angular dispersion and maintain better beam alignment. The primary benefit of these simulations is to help create efficient VLC access point coverage plans throughout standard indoor areas.

5. CONCLUSIONS

In this paper, we have developed a collaborative hybrid VLC/RF system and solutions through a MIMO structure. Improved data transmission in the system with the optical devices' ultrahigh bandwidths and RF robustness in industrial environments that require secure and stronger data transfer.

The research considered some vital factors such as OOK modulation, BER analysis, and the received optical power distribution, multiuser access system, as well as the hybrid VLC/Wi-Fi network system. The performance of the system was enhanced using frequency reuse planning and Shannon spectral efficiency techniques.

The system gets practical use by using VLC downlink and RF uplink communications for applications involving Cobots and IIoT systems. The arrangement prevents visual discomfort from the source of lighting and increases system consistency at the same time. The results show that the hybrid VLC-RF system provides an effective solution to provide rapid and safe wireless communication in industrial environments in the smart age. Future work will focus on enhancing the robustness, scalability, and security of hybrid VLC/RF systems through advanced noise modelling, latency analysis, adaptive resource allocation, failure recovery, and experimental validation in realistic industrial environments.

ACKNOWLEDGEMENT

This work is supported by the Ministry of Higher Education and Scientific Research of Algeria.

REFERENCES

[1] Ghassemlooy, Z., Zvanovec, S., Khalighi, M.A., Popoola, W.O., Perez, J. (2017). Optical wireless communication

systems. Optik - International Journal for Light and Electron Optics, 151: 1-6. https://doi.org/10.1016/j.ijleo.2017.11.052

[2] Kwon, J. (2023). A study on ethical awareness changes and education in artificial intelligence society. Revue d'Intelligence Artificielle, 37(2): 341-345. https://doi.org/10.18280/ria.370212

[3] Patel, K., Patel, P., Sonawane, C., Bongale, A.K., Tejani, G.G., et al. (2025). Design and evaluation of a parallel manipulator for interconnected transmission tracking. Mathematical Modelling of Engineering Problems, 12(5): 1615-1626. https://doi.org/10.18280/mmep.120516

[4] Faura-Pujol, A., Faundez-Zanuy, M., Moral-Viñals, A., López-Xarbau, J. (2023). Eye-tracking calibration to control a cobot. International Journal of Computational Methods and Experimental Measurements, 11(1): 17-25. https://doi.org/10.18280/ijcmem.110103

[5] Chaabna, A., Babouri, A., Huang, C., Zhang, X., Chouabia, H. (2020). New indoor positioning technique using spectral data compression based on VLC for performance improvement. Optical and Quantum Electronics, 52(7): 1-21. https://doi.org/10.1007/s11082-020-02452-z

[6] Chaabna, A., Babouri, A., Huang, C., Zhang, X. (2019). Visible light communication system for indoor positioning using solar cell as receiver. International Journal of Energy Optimization and Engineering (IJEOE), 8(2): 47-60. https://doi.org/10.4018/IJEOE.2019040103

[7] Basnayaka, D.A., Haas, H. (2017). Design and analysis of a hybrid radio frequency and visible light communication system. IEEE Transactions on Communications, 65(10): 4334-4347. https://doi.org/10.1109/TCOMM.2017.2702177

[8] Chedup, S., Subba, B., Dorji, S., Perera, T.D.P., Rajaram, A., Jayakody, D.N.K. (2018). Visible light energy harvesting in modern communication systems. In IEEE International Conference on Electrical, Electronics, Computers, Communication, Mechanical and Computing (EEC-CMC), Priyadarshini Engineering College, India, pp. 1-8.

[9] Basnayaka, D.A., Haas, H. (2015). Hybrid RF and VLC systems: Improving user data rate performance of VLC systems. In 81st IEEE Vehicular Technology Conference, VTC Spring 2015, Glasgow, United Kingdom, pp. 1-5. https://doi.org/10.1109/VTCSpring.2015.7145863

[10] Kafafy, M., Fahmy, Y., Abdallah, M., Khairy, M. (2017). Power efficient downlink resource allocation for hybrid RF/VLC wireless networks. In Wireless Communications and Networking Conference (WCNC), San Francisco, CA, USA, pp. 1-6. https://doi.org/10.1109/WCNC.2017.7925892

[11] Li, Z., Shao, S., Khreishah, A., Ayyash, M., Abdalla, I., Elgala, H., Rahaim, M., Little, T. (2018). Design and implementation of a hybrid RF-VLC system with bandwidth aggregation. In 14th International Wireless Communications and Mobile Computing Conference, IWCMC 2018 - Limassol, Cyprus, pp. 194-200. https://doi.org/10.1109/IWCMC.2018.8450350

[12] Manogna, A., Bhat, A.V., Patil, B.M., Krithika, K.C., Surendra, H.H. (2020). Analysis of Bluetooth, Wi-Fi, ZigBee and VLC. International Journal of Advanced Research in Electrical, Electronics and Instrumentation Engineering (IJAREEIE), 9(6): 1473-1480. https://www.ijareeie.com/upload/2020/june/37_Analysis_NC.PDF?utm_source=chatgpt.com.

[13] Abdel Momen, M.M., Fayed, H.A., Aly, M.H., Ismail, N.E., Mokhtar, A. (2019). An efficient hybrid visible light communication / radio frequency system for vehicular applications. Optical and Quantum Electronics, 51(11): 1-24. https://doi.org/10.1007/s11082-019-2082-7

[14] Chowdhury, M.Z., Hossan, Md. T., Hasan, M.K., Jang, Y.M. (2011). Integrated RF/optical wireless networks for improving QoS in indoor and transportation applications. Wireless Personal Communications, 107: 1401-1430. https://doi.org/10.1007/s11277-018-5971-3

[15] Stefan, I., Haas, H. (2014). A hybrid radio frequency and broadcast visible light communication system. In IEEE 80th Vehicular Technology Conference (VTC2014-Fall), Vancouver, BC, Canada, pp. 1-5. https://doi.org/10.1109/VTCFall.2014.6965999

[16] Ashok, A. (2017). Hybrid VLC and radio communication: Potential, challenges and solutions for coexistence. In Proceedings of the 4th ACM Workshop on Visible Light Communication Systems (VLCS '17). In Association for Computing Machinery, New York, USA, pp. 1-49. https://doi.org/10.1145/3129881.3139223

[17] Yadav, B., Patel, P. (2025). Adaptive power allocation design of beyond 6G highly dense NOMA-Massive MIMO infinity-norm box detection technique. Traitement du Signal, 42(1): 101-118. https://doi.org/10.18280/ts.420110

[18] Zeng, L., O'Brien, D.C., Le Minh, H., Faulkner, G.E., Lee, K.W., et al. (2009). High data rate multiple input multiple output (MIMO) optical wireless communications using white LED lighting. IEEE Journal on Selected Areas in Communications, 27(9): 1654-1662. https://doi.org/10.1109/JSAC.2009.091215

[19] Jungnickel, V., Pohl, V., Nonning, S., Von Helmolt, C. (2002). A physical model of the wireless infrared communication channel. IEEE Journal on Selected Areas in Communications, 20(3): 631-640. https://doi.org/10.1109/49.995522

[20] Kahn, J.M., Barry, J.R. (1997). Wireless infrared communications. Proceedings of the IEEE, 85(2): 265-298. https://doi.org/10.1109/5.554222

[21] Wang, Y., Videv, S., Haas, H. (2014). Dynamic load balancing with handover in hybrid Li-Fi and Wi-Fi networks. In 2014 IEEE 25th Annual International Symposium on Personal, Indoor, and Mobile Radio Communication (PIMRC), Washington, DC, USA, pp. 575-579. https://doi.org/10.1109/PIMRC.2014.7136231

[22] Wang, Y., Wu, X., Haas, H. (2016). Fuzzy logic based dynamic handover scheme for indoor Li-Fi and RF hybrid network. In 2016 IEEE International Conference on Communications (ICC), Kuala Lumpur, Malaysia, pp. 1-6. https://doi.org/10.1109/ICC.2016.7510823

[23] Tse, D., Viswanath, P. (2005). Fundamentals of wireless communication. Cambridge University Press, New York. https://doi.org/10.1017/CBO9780511807213

[24] Cox, D.C., Murray, R.R., Norris, A.W. (1983). Measurements of 800MHz radio transmission into buildings with metallic walls. In The Bell System Technical Journal, 62(9): 2695-2717. http://doi.org/10.1002/j.1538-7305.1983.tb03200.x

[25] Alexander, S.E. (1982). Radio propagation within buildings at 900MHz. Electronics Letters, 18(21): 913-914. https://doi.org/10.1049/el:19820622
[26] Rappaport, S. (2002). Wireless Communications: Principles and Practice. New Jersey, Prentice Hall, 122-128.
[27] Pechac, P., Klepal, M. (2000). Empirical models for indoor propagation in CTU Prague buildings. Radio Engineering, 9(1): 31-36.
[28] Haas, H., Yin, L., Wang, Y., Chen, C. (2016). What is LiFi? Journal of Lightwave Technology, 34(6): 1533-1544. https://doi.org/10.1109/JLT.2015.2510021